Adobe Photoshop 4.0, Adobe Streamline 3.0 and Strata Studio Pro 2.5.3. We used the following primary antibodies: rabbit anti-Frazzled[3] (1:500 dilution); goat anti-Netrin-B[18] (1:500); rabbit anti-β-galactosidase (1:2,000, Cappel), goat anti-HRP (1:2,000, Cappel), monoclonal antibody 22C10 (ref. 30; 1:20, from Developmental Studies Hybridoma Bank (DSHB)), rabbit anti-GFP (1:100, Clontech); monoclonal antibody anti-Myc 9E10 (1:10, developed by J. M. Bishop, obtained from DSHB). Mutant embryos were identified using balancer chromosomes carrying β-galactosidase genes, or by staining with anti-Frazzled antibody (Fig. 2f, 4b) or anti-Netrin-B antibody (Fig. 3b). The rescue of the dMP2 phenotype by Frazzled expression in and outside dMP2 (Fig. 3j–m) was judged using the following criteria. To show the presence of the mutant phenotype (Fig. 3k, l), we scored the dMP2 pathway as abnormal if the $22C10^+$ fascicle was discontinuous at the segmental boundary. To demonstrate phenotypic rescue when Frazzled was expressed outside dMP2 (Fig. 3m), we scored as phenotypically normal hemisegments that had both of the following properties: (1) $22C10^+$ fascicle was present at the segmental boundary; and (2) an axon with dMP2-specific morphology was present after it has passed the segmental boundary. These criteria were chosen because there are several $22C10^+$ axons within the dMP2 fascicle at the segmental boundary. Our criteria underestimate both the dMP2 defect in Fig. 3k, l and the rescue of the phenotype in Fig. 3m.

Received 2 February; accepted 22 May 2000.

1. Serafini, T. *et al.* The netrins define a family of axon outgrowth-promoting proteins homologous to *C. elegans* UNC-6. *Cell* **78,** 409–424 (1994).
2. de la Torre, J. R. *et al.* Turning of retinal growth cones in a netrin-1 gradient mediated by the netrin receptor DCC. *Neuron* **6,** 1211–1224 (1997).
3. Kolodziej, P. A. *et al. frazzled* encodes a *Drosophila* member of the DCC immunoglobulin subfamily and is required for CNS and motor axon guidance. *Cell* **87,** 197–204 (1996).
4. Chan, S. S. *et al.* UNC-40, a *C. elegans* homolog of DCC (Deleted in Colorectal Cancer), is required in motile cells responding to UNC-6 netrin cues. *Cell* **87,** 187–195 (1996).
5. Keino-Masu, K. *et al.* Deleted in Colorectal Cancer (DCC) encodes a netrin receptor. *Cell* **87,** 175–185 (1996).
6. Leung-Hagesteijn, C. *et al.* UNC-5, a transmembrane protein with immunoglobulin and thrombospondin type 1 domains, guides cell and pioneer axon migrations in *C. elegans*. *Cell* **71,** 289–299 (1992).
7. Hamelin, M., Zhou, Y., Su, M. W., Scott, I. M. & Culotti, J. G. Expression of the UNC-5 guidance receptor in the touch neurons of *C. elegans* steers their axons dorsally. *Nature* **364,** 327–330 (1993).
8. Ackerman, S. L. *et al.* The mouse rostral cerebellar malformation gene encodes an UNC-5-like protein. *Nature* **386,** 838–842 (1997).
9. Leonardo, E. D. *et al.* Vertebrate homologues of *C. elegans* UNC-5 are candidate netrin receptors. *Nature* **386,** 833–838 (1997).
10. Fazeli, A. *et al.* Phenotype of mice lacking functional Deleted in colorectal cancer (Dcc) gene. *Nature* **386,** 796–804 (1997).
11. Przyborski, S. A., Knowles, B. B. & Ackerman, S. L. Embryonic phenotype of Unc5h3 mutant mice suggests chemorepulsion during the formation of the rostral cerebellar boundary. *Development* **125,** 41–50 (1998).
12. Hong, K. *et al.* A ligand-gated association between cytoplasmic domains of UNC5 and DCC family receptors converts netrin-induced growth cone attraction to repulsion. *Cell* **97,** 927–941 (1999).
13. Bashaw, G. J. & Goodman, C. S. Chimeric axon guidance receptors: the cytoplasmic domains of slit and netrin receptors specify attraction versus repulsion. *Cell* **97,** 917–926 (1999).
14. Gong, Q., Rangarajan R., Seeger, M. & Gaul, U. The Netrin receptor Frazzled is required in the target for establishment of retinal projections in the *Drosophila* visual system. *Development* **126,** 1451–1456 (1999).
15. Serafini, T. *et al.* Netrin-1 is required for commissural axon guidance in the developing vertebrate nervous system. *Cell* **87,** 1001–1014 (1996).
16. Kennedy, T. E., Serafini, T., de la Torre, J. R. & Tessier-Lavigne, M. Netrins are diffusible chemotropic factors for commissural axons in the embryonic spinal cord. *Cell* **78,** 425–435 (1994).
17. Mitchell, K. J. *et al.* Genetic analysis of Netrin genes in *Drosophila*: Netrins guide CNS commissural axons and peripheral motor axons. *Neuron* **17,** 203–215 (1996).
18. Harris, R., Sabatelli, L. M., & Seeger, M. A. Guidance cues at the *Drosophila* CNS midline: identification and characterization of two *Drosophila* Netrin/UNC-6 homologs. *Neuron* **17,** 217–228 (1996).
19. Hedgecock, E. M., Culotti, J. G. & Hall, D. H. The unc-5, unc-6, and unc-40 genes guide circumferential migrations of pioneer axons and mesodermal cells on the epidermis in *C. elegans*. *Neuron* **4,** 61–85 (1990).
20. Wadsworth, W. G., Bhatt, H. & Hedgecock, E. M. Neuroglia and pioneer neurons express UNC-6 to provide global and local netrin cues for guiding migrations in *C. elegans*. *Neuron* **16,** 35–46 (1996).
21. Ishii, N., Wadsworth, W. G., Stern, B. D., Culotti, J. G. & Hedgecock, E. M. UNC-6, a laminin-related protein, guides cell and pioneer axon migrations in *C. elegans*. *Neuron* **9,** 873–881 (1992).
22. Colamarino, S. A. & Tessier-Lavigne, M. The axonal chemoattractant netrin-1 is also a chemorepellent for trochlear motor axons. *Cell* **81,** 621–629 (1995).
23. Brose, K. *et al.* Slit proteins bind Robo receptors and have an evolutionarily conserved role in repulsive axon guidance. *Cell* **96,** 795–806 (1999).
24. Jacobs, J. R. & Goodman, C. S. Embryonic development of axon pathways in the *Drosophila* CNS. II. Behavior of pioneer growth cones. *J. Neurosci.* **9,** 2412–2422 (1989).
25. Hidalgo, A. & Brand, A. H. Targeted neuronal ablation: the role of pioneer neurons in guidance and fasciculation in the CNS of *Drosophila*. *Development* **124,** 3253–3262 (1997).
26. Ramírez-Weber, F. A. & Kornberg, T. B. Cytonemes: cellular processes that project to the principal signaling center in *Drosophila* imaginal discs. *Cell* **97,** 599–607 (1999).
27. Winberg, M. L., Mitchell, K. J. & Goodman, C. S. Genetic analysis of the mechanisms controlling target selection: complementary and combinatorial functions of netrins, semaphorins, and IgCAMs. *Cell* **93,** 581–591 (1998).
28. Brand, A. H. & Perrimon, N. Targeted gene expression as a means of altering cell fates and generating dominant phenotypes. *Development* **118,** 401–415 (1993).
29. Ashburner, M. *Drosophila, a Laboratory Manual.* (CSHL, Cold Spring Harbor, 1989).
30. Fujita, S. C., Zipursky, S. L., Benzer, S., Ferrus, A. & Shotwell, S. L. Monoclonal antibodies against the *Drosophila* nervous system. *Proc. Natl Acad. Sci. USA* **79,** 7929–7933 (1982).

Acknowledgements

We thank A. Chiba, C. S. Goodman, A. Hidalgo, P. Kolodziej, M. Seeger and G. Technau for fly strains; P. Kolodziej and M. Seeger for DNA clones and antibodies; T. Hosoya, Y. Umesono, M. Okabe and all members of the Hotta laboratory for helpful discussions; and Y. Fujioka, M. Seki, M. Sakai and C. Asaka for technical assistance. This work was funded by CREST (Y. Hotta and Y. Hiromi), the Ministry of Education, Science, Sports, and Culture of Japan, and Research for the Future Program of JSPS (Y. Hiromi) and NIH (E.G.).

Correspondence and requests for materials should be addressed to Y.H. (e-mail: yhotta@lab.nig.ac.jp).

Intracellular calcium dependence of transmitter release rates at a fast central synapse

Ralf Schneggenburger & Erwin Neher

Abteilung Membranbiophysik, Max-Planck-Institut für biophysikalische Chemie, Am Fassberg 11, D-37077 Göttingen, Germany

Calcium-triggered fusion of synaptic vesicles and neurotransmitter release are fundamental signalling steps in the central nervous system. It is generally assumed that fast transmitter release is triggered by elevations in intracellular calcium concentration ($[Ca^{2+}]_i$) to at least 100 μM near the sites of vesicle fusion[1–5]. For synapses in the central nervous system, however, there are no experimental estimates of this local $[Ca^{2+}]_i$ signal. Here we show, by using calcium ion uncaging in the large synaptic terminals of the calyx of Held, that step-like elevations to only 10 μM $[Ca^{2+}]_i$ induce fast transmitter release, which depletes around 80% of a pool of available vesicles in less than 3 ms. Kinetic analysis of transmitter release rates after $[Ca^{2+}]_i$ steps revealed the rate constants for calcium binding and vesicle fusion. These show that transient (around 0.5 ms) local elevations of $[Ca^{2+}]_i$ to peak values as low as 25 μM can account for transmitter release during single presynaptic action potentials. The calcium sensors for vesicle fusion are far from saturation at normal release probability. This non-saturation, and the high intracellular calcium cooperativity in triggering vesicle fusion, make fast synaptic transmission very sensitive to modulation by changes in local $[Ca^{2+}]_i$.

The rapidly decaying, local $[Ca^{2+}]_i$ signal that triggers vesicle fusion in presynaptic terminals cannot readily be resolved with current imaging techniques. To circumvent this problem, we applied Ca^{2+} uncaging in large presynaptic terminals, the calyces of Held[6,7], located in the brainstem medial nucleus of the trapezoid body. During Ca^{2+} uncaging, cytosolic $[Ca^{2+}]_i$ is elevated in a spatially homogenous manner[8]. Therefore, fluorescent Ca^{2+} indicators can be used to measure directly the biologically relevant $[Ca^{2+}]_i$ acting at the sensor for vesicle fusion[9,10].

Calyces were loaded through whole-cell patch pipettes with mixtures of the photolysable Ca^{2+} chelator DM-nitrophen (1 mM) and the low-affinity fluorescent Ca^{2+} indicator fura-2 FF (Fig. 1a). The transmitter release activity was monitored by recording excitatory postsynaptic currents (EPSCs) from principal neurons with a second patch pipette (Fig. 1a). Cyclothiazide (CTZ; 100 μM) was present during most recordings to suppress the desensitization[11,12] of AMPA (α-amino-3-hydroxy-5-methyl-4-isoxazole propionic acid)-type glutamate receptors, which mediate fast EPSCs in these synapses.

We used flashes of varying intensities to study the magnitude of the postsynaptic response as a function of presynaptic $[Ca^{2+}]_i$. Dim flashes that elevated $[Ca^{2+}]_i$ to about 2 μM (Fig. 1b, blue trace) evoked small postsynaptic currents in which individual quantal events could be identified (Fig. 1c). Stronger flashes, which elevated the presynaptic $[Ca^{2+}]_i$ to roughly two- or threefold higher values (Fig. 1b, red and black traces), caused much larger EPSCs, in which individual quantal events were no longer detectable (Fig. 1d). Stable flash responses could be observed several times in a given cell pair. This is shown in Fig. 1d, in which the black and the grey trace, respectively, represent the response to the first and the seventh flash, which evoked similar presynaptic $[Ca^{2+}]_i$ changes and similar EPSCs. These large EPSCs reflect the release activity of several hundred active zones that operate in parallel at calyx of Held synapses[13,14].

To quantify transmitter release rates, we deconvolved the multiquantal EPSC responses with the quantal response waveform[15,16]. This was necessary because peak EPSC amplitudes are not a valid measure of transmitter release, unless release is highly synchronized. We estimated the quantal response waveforms by recording spontaneous miniature EPSCs (mEPSCs) under the same conditions as flash-evoked EPSCs. Average mEPSC traces (Fig. 1f) had amplitudes of 33 ± 9.3 pA, and their decay was biphasic, with fast and slow time constants of 1.9 ± 0.4 and 13.4 ± 2.6 ms, respectively ($n = 5$ cells). The deconvolution of flash-evoked, compound EPSCs therefore assumed such quantal response waveforms with double-exponential decays (see Methods). Deconvolution revealed peak release rates of about 10 and 60 quanta per ms (see Fig. 1e) for the flash-evoked, multiquantal EPSCs shown in Fig. 1d.

In experiments with a higher DM-nitrophen concentration (2 mM), step-like elevations of up to 25 μM $[Ca^{2+}]_i$ were produced (see Fig. 1g), which evoked larger EPSCs with faster rise times. EPSCs reached maximal amplitudes at $[Ca^{2+}]_i \approx 12$ μM. Increasing $[Ca^{2+}]_i$ further caused a speeding of the rising phase, but did not alter the amplitude of EPSCs (compare black and red traces in Fig. 1h). The corresponding integrated release rate traces (Fig. 1i, dashed lines) show that at $[Ca^{2+}]_i > 12$ μM, cumulative release was similar within around 3 ms after the onset of release, indicating that a pool of readily releasable vesicles[14,17] may have been depleted by such $[Ca^{2+}]_i$ steps. The late (>3 ms) slow rise in the integrated release rate traces may be due to inaccuracies in the release rate estimates during the decaying phase of EPSCs (Fig. 1h, i) or to a genuine slow component of transmitter release. A small effect of postsynaptic receptor saturation on the peak EPSC amplitudes of the largest responses cannot be excluded. This, however, should not affect our estimate of peak release rates, as these occur at the point of the steepest rise of EPSCs, before the EPSCs reach their peak amplitudes (Fig. 1h, i).

We next tested whether Ca^{2+} uncaging and the $[Ca^{2+}]_i$ signal created by the opening of voltage-gated Ca^{2+} channels induce vesicle fusion from a common pool of readily releasable vesicles. We studied the inhibition of depolarization-induced EPSCs by preceding flash-evoked transmitter release (Fig. 2)[14]. In the example shown in Fig. 2, a depolarization-evoked Ca^{2+} current induced a control EPSC of 25.8 nA (Fig. 2b, black trace), which was reduced to 18.1 nA (Fig. 2b, blue trace) and 4.4 nA (Fig. 2b, red trace) when the depolarizing pulses were preceded by flashes of varying intensities. This inhibition was not accompanied by a reduction in presynaptic Ca^{2+} currents (I_{Ca} was 97 ± 5% of control after flashes; $n = 9$). Half-maximal and 80% inhibition occurred with $[Ca^{2+}]_i$ steps of around

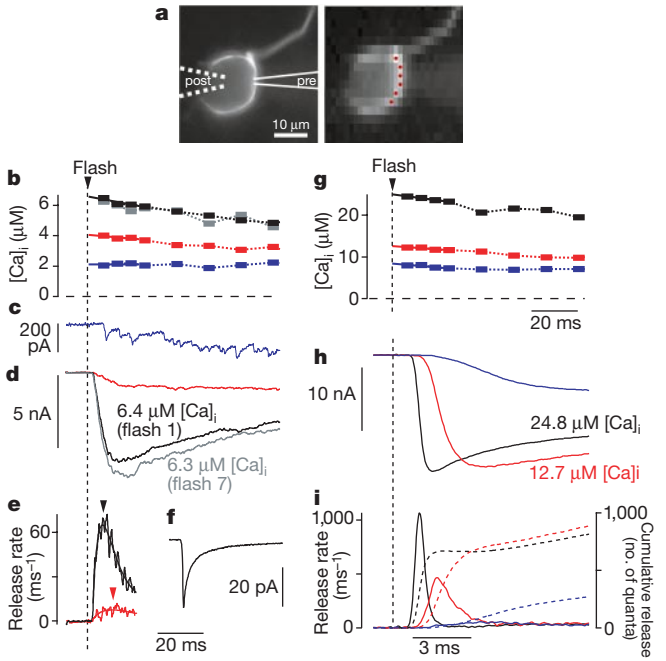

Figure 1 Presynaptic $[Ca^{2+}]$ steps and postsynaptic detection of transmitter release. **a**, Fluorescent images at 380 nm excitation of a calyx of Held nerve terminal filled through a whole-cell patch pipette with Ca^{2+} indicator, fura-2 FF and photolysable Ca^{2+} chelator, DM-nitrophen (1 mM). Red dots indicate binned pixels used for the analysis of cellular fluorescence changes. **b**, Elevations of presynaptic $[Ca^{2+}]_i$, obtained by light flashes with different transmission intensities. **c**, **d**, EPSCs in response to the presynaptic $[Ca^{2+}]_i$ elevations shown in **b**. Colours identify corresponding $[Ca^{2+}]_i$, EPSC and release rate traces in **b**–**e**. **e**, Transmitter release rates obtained from deconvolution of two EPSCs shown in **d**. **f**, An averaged mEPSC trace from 436 individual traces. **g**–**i**, Presynaptic $[Ca^{2+}]_i$ elevations (**g**), EPSCs (**h**) and transmitter release rates (**i**) for a different cell pair. In **i**, cumulative release rates (dashed lines) were obtained by integrating the corresponding release rate traces.

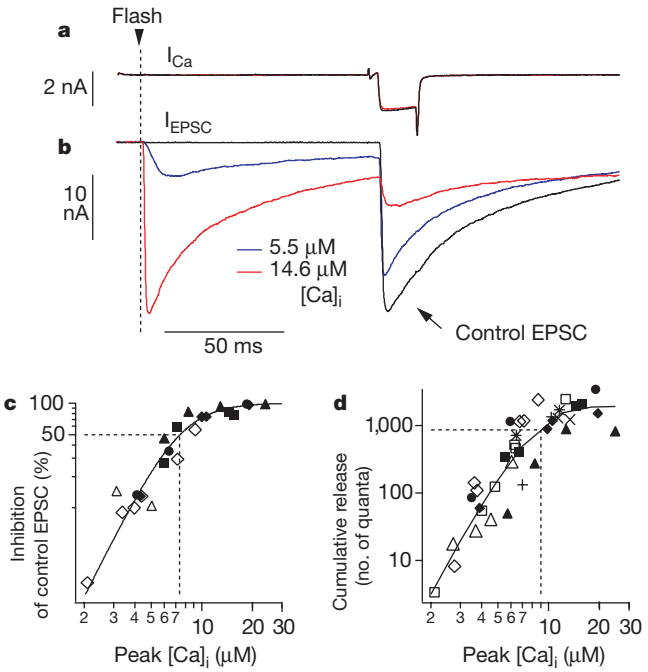

Figure 2 $[Ca^{2+}]_i$ elevations induced by flashes and presynaptic depolarizations release vesicles from a common pool. **a**, Presynaptic Ca^{2+} currents (I_{Ca}) under control conditions (black trace) and after a flash (red trace). Ca^{2+} currents were evoked by a 4-μs depolarization to +80 mV, followed by a 16-ms period at 0 mV. **b**, EPSCs corresponding to the traces shown in **a**. The blue and red traces were obtained after flashes that elevated the presynaptic $[Ca^{2+}]_i$ to the indicated levels. **c**, Inhibition of depolarization-evoked EPSCs as a function of flash-induced presynaptic $[Ca^{2+}]_i$. Half-maximal inhibition occurred at ~7 μM $[Ca^{2+}]_i$, as indicated by a Hill-function fit of the data (solid line). **d**, Cumulative transmitter release, analysed for $n = 10$ cells by integrating the release rates in a 10-ms interval (Fig. 1i). The predictions of the model shown in Fig. 3e are superimposed (solid line).

7 and 10 μM, respectively (Fig. 2c). Figure 2d shows the $[Ca^{2+}]_i$ dependence of cumulative transmitter release, obtained by integrating the release rates over the first 10 ms after flashes (see Fig. 1i). The inhibition of depolarization-induced EPSCs (Fig. 2c) and the cumulative transmitter release (Fig. 2d) showed almost identical $[Ca^{2+}]_i$ dependencies. This indicates that both types of Ca^{2+} stimulus draw upon the same pool of rapidly releasable (<10 ms) vesicles. Cumulative release reached a plateau of 1,785 ± 870 released quanta with $[Ca^{2+}]_i$ steps above 12 μM (n = 8 flashes; see Fig. 2d). This number is larger than a previous pool size estimate based on analysing EPSC charges in the absence of CTZ[14], perhaps owing to a contribution of AMPA-receptor desensitization[12] in the previous study. Nevertheless, the pool size estimates showed considerable scatter between cells (range 800–3,500; see Fig. 2d).

Figure 3a shows the $[Ca^{2+}]_i$ dependence of transmitter release rates, measured from 47 flash responses in 13 cell pairs. In the range 2–8 μM $[Ca^{2+}]_i$, peak release rates increased as a power function of $[Ca^{2+}]_i$, with an exponent of 4.2, as indicated by linear regression analysis in the double-logarithmic plot of Fig. 3a. This exponent is similar to previous values obtained by varying the extracellular Ca^{2+} concentration at neuromuscular junction synapses[18] or at central synapses, including the calyx of Held[13,14]. At values above 10 μM, release rates increased with a more shallow dependency on $[Ca^{2+}]_i$. In the range 8–13 μM $[Ca^{2+}]_i$, the average release rate was 349 ± 209 ms^{-1} (n = 9 flashes), a value similar to the peak release rates measured during action-potential-evoked EPSCs (see below; Fig. 4). Nevertheless, the corresponding average $[Ca^{2+}]_i$ (10.7 ± 1.5 μM) is not necessarily equal to the peak $[Ca^{2+}]_i$ reached at the Ca^{2+} sensors for vesicle fusion during a single presynaptic action potential. This is because the local $[Ca^{2+}]_i$ signal during an action potential probably decays very rapidly, which might curtail transmitter release before Ca^{2+} binding to the sensor for vesicle fusion reaches equilibrium.

To learn about the rate-limiting steps involved in Ca^{2+}-dependent vesicle fusion at the calyx of Held synapse, we fitted the flash-photolysis data with a minimal kinetic model, incorporating several Ca^{2+}-binding steps, followed by vesicle fusion from the fully Ca^{2+}-bound state[4,10] (Fig. 3e). As it has been reported[19] that uncaging of Ca^{2+} by flash photolysis can, under certain conditions, lead to brief (~1–2 ms) spike-like overshoots of $[Ca^{2+}]_i$ that would have been undetected by Ca^{2+} imaging, we first modelled the expected $[Ca^{2+}]_i$ time course after flash photolysis (see Methods). The resulting $[Ca^{2+}]_i$ time course (Fig. 3d) did not show a significant spike. This is attributable to the almost full loading of DM-nitrophen with Ca^{2+}, and to rapid Ca^{2+} buffering by ATP and by endogenous Ca^{2+} buffers. The calculated $[Ca^{2+}]_i$ time course was then used to drive the Ca^{2+}-binding scheme shown in Fig. 3e. To predict the high initial slope of 4.2 in the double-logarithmic plot of release rates versus $[Ca^{2+}]_i$ (Fig. 3a), it was necessary to include five Ca^{2+}-binding steps, as well as a cooperativity factor[4] (b in the scheme of Fig. 3e).

The analysis of synaptic delays (Fig. 3b) and times to peak release (Fig. 3c) gave important constraints for setting the Ca^{2+}-binding and -unbinding rate constants. When these rate constants were increased, a good fit of the peak release rates (Fig. 3a) was still obtained, but the delays and times to peak release (Fig. 3b, c) were then significantly underestimated at low $[Ca^{2+}]_i$ (data not shown). The set of parameters found by fitting the data in Fig. 3 also accurately predicted the decrease in cumulative transmitter release with submaximal $[Ca^{2+}]_i$ elevations (Fig. 2d). Note, however, that the value of the vesicle fusion rate γ is only a lower limit estimate because the finite rising speed of mEPSCs, as well as possible postsynaptic receptor saturation, might contribute to the apparent levelling-off of peak release rates at $[Ca^{2+}]_i > 10$ μM.

Knowledge of the kinetic parameters of Ca^{2+} binding and vesicle fusion (Fig. 3) should allow us to infer the time course and amplitude of the local $[Ca^{2+}]_i$ signal during transmitter release

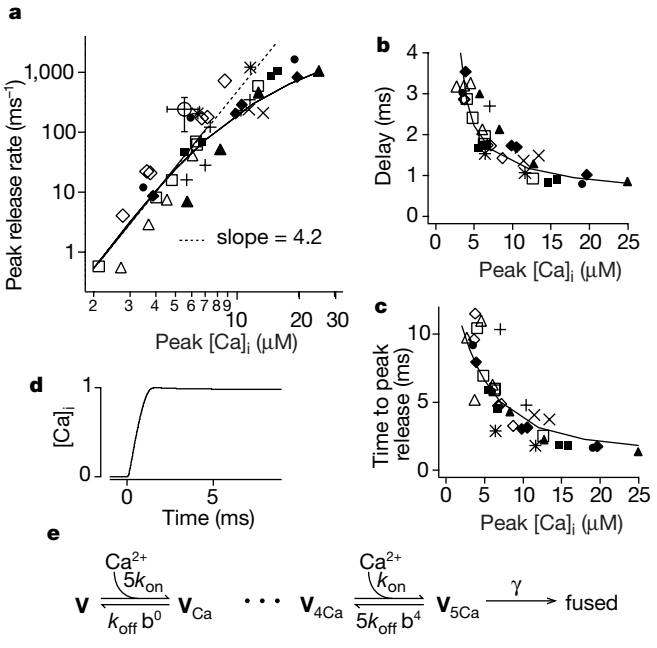

Figure 3 Intracellular Ca^{2+} concentration dependence of transmitter release rates at the calyx of Held synapse. **a**, Peak release rates as a function of presynaptic $[Ca^{2+}]_i$ after flash photolysis. Data from n = 10 cells with either 1 mM (open symbols) or 2 mM DM-nitrophen (filled symbols). The open round symbol represents average results (n = 3 cells) with NP-EGTA as photolysable Ca^{2+} chelator (see Methods). Data from experiments in the absence of CTZ (star-like symbols; n = 2) is also shown. The dashed line indicates a slope of 4.2. **b**, Delay between the time of flash trigger (t = 0), and occurrence of first transmitter release. **c**, Time to reach peak release rates (see Fig. 1e, arrowheads). In **a**–**c**, predictions of the kinetic model (**e**) are shown by solid lines. **d**, Simulation of the $[Ca^{2+}]_i$ time course after flash photolysis. **e**, Scheme of a kinetic model used to fit the data. The following parameters were found: k_{on}, 9×10^7 M^{-1} s^{-1}; k_{off}, 9,500 s^{-1}; γ, 6,000 s^{-1}; b = 0.25.

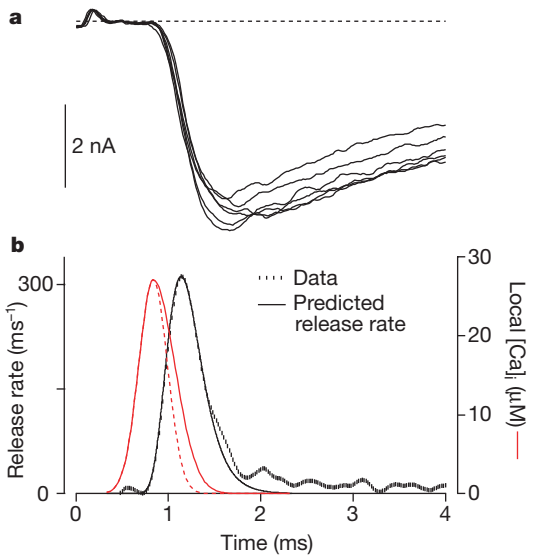

Figure 4 The predicted local $[Ca^{2+}]_i$ signal at an average Ca^{2+} sensor for vesicle fusion during single presynaptic action potentials. **a**, Six consecutive EPSCs evoked by fibre stimulation (0.05 Hz) in the presence of 2 mM Ca^{2+}, 1 mM Mg^{2+} and 100 μM CTZ. **b**, Average transmitter release rates obtained by deconvolution of the EPSCs in **a**. Red line, inferred local $[Ca^{2+}]_i$ signal that predicts a release rate (black line) similar to that observed. Dashed red curve, gaussian with half-width of 0.36 ms, an idealized representation of the Ca^{2+} current waveform[13] during a single action potential at the calyx of Held.

triggered by presynaptic action potentials. To do so, we first measured transmitter release rates during EPSCs evoked by afferent fibre stimulation. Six consecutive EPSCs, obtained in the presence of 100 μM CTZ, are shown in Fig. 4a on an expanded time scale. The addition of CTZ to the bath solution increased peak EPSC amplitudes by 17.7 ± 11.1% ($n = 4$), an effect that is probably caused by the more effective peak summation of mEPSCs with slowed decay times in the presence of CTZ (but see refs 16 and 20). The EPSCs were deconvolved with quantal response waveforms, which were obtained by sampling spontaneous mEPSCs between single fibre stimulations for each cell. The average peak release rate was 335 ± 111 ms^{-1} ($n = 4$ cells). The duration of transmitter release at half-maximal amplitude was 0.44 ± 0.07 ms (Fig. 4b), in good agreement with a previous estimate obtained from delay histograms[13].

We next set out to calculate the local $[Ca^{2+}]_i$ signal that an average vesicle might experience during a presynaptic action potential. As a starting point we assumed this signal to be proportional to the Ca^{2+} current measured during action potentials at the calyx of Held[13]. This implies that the local $[Ca^{2+}]_i$ transient is produced by overlap of $[Ca^{2+}]_i$ domains created by several neighbouring Ca^{2+} channels within a short distance. We then performed model calculations with the kinetic parameters obtained from the flash data (Fig. 3), and varied the decay and the amplitude of the local $[Ca^{2+}]_i$ waveform to obtain adequate predictions of transmitter release during action potentials. In four cells with average EPSC amplitudes of 5.88 ± 4 nA, we found $[Ca^{2+}]_i$ transients with peak amplitudes of 27.8 ± 1.4 μM and half-widths of 0.46 ± 0.05 ms. The width at half-amplitude of the inferred local $[Ca^{2+}]_i$ signal exceeded that of presynaptic Ca^{2+} currents during action potentials[13] by only ~100 μs (Fig. 4b, compare solid and dashed red lines), indicating that fast processes such as diffusion or binding to endogenous Ca^{2+} buffers[3,5] must be extremely effective in terminating the local $[Ca^{2+}]_i$ signal after Ca^{2+} channels close.

We have shown that the fast phase of transmitter release at a central nervous system (CNS) synaptic terminal occurs at $[Ca^{2+}]_i$ values that are significantly lower than the range of 75–300 μM predicted by theoretical studies[3,5], by experiments on invertebrate synapses[1,2,19] or by flash photolysis in retinal bipolar cell terminals[4]. In ref. 4, secretion measured by membrane capacitance was absent below 10–20 μM $[Ca^{2+}]_i$ (but see ref. 21), a Ca^{2+} concentration at which we observe strong transmitter release from calyces, at rates equalling those obtained with single action potentials (Fig. 3a). It is possible that ribbon-type synapses found in sensory systems have vesicle fusion mechanisms with a lower Ca^{2+} sensitivity than those at the calyx of Held synapse with its conventional active zones. It is usually assumed that fast synaptic transmission is driven by rapid local $[Ca^{2+}]_i$ transients to values above 100 μM, which might be found in the immediate vicinity (< 10 nm) of an open Ca^{2+} channel[3,5]. Our data show that fast vesicle fusion can occur at much lower peak $[Ca^{2+}]_i$ during single action potentials (~25 μM; Fig. 4b), indicating that tight (<10 nm) molecular coupling of vesicles and Ca^{2+} channels at this synapse is not necessary for fast transmitter release. This conclusion is supported by the finding that presynaptic injection of EGTA, a Ca^{2+} buffer with a slow binding rate, reduces EPSC amplitudes at this[13] and at neocortical synapses[22], again implying that a significant contribution to the local $[Ca^{2+}]_i$ signal originates from remote channels. The possibility that the colocalization of vesicles and Ca^{2+} channels becomes more tight with maturation of synapses can, however, not be excluded at present. In any case, the local $[Ca^{2+}]_i$ at the sensors for vesicle fusion is about fifty times higher than the spatially averaged $[Ca^{2+}]_i$ attained with single action potentials (~0.5 μM)[23], confirming the significance of spatially localized $[Ca^{2+}]_i$ signals for synaptic transmission[1–5].

Action potentials released 178 ± 86 quanta ($n = 4$ cells) within 2 ms (Fig. 4), corresponding to roughly 10% of the pool of readily releasable vesicles as determined in Fig. 2. This rather small released fraction, which is at the lower limit of previous estimates at this synapse[14,17], is a typical feature of CNS synapses[24]. Sustained $[Ca^{2+}]_i$ elevations to 25 μM (Fig. 1g, h, i; black traces) lead to transmitter release rates several times larger than those observed with single presynaptic action potentials (Fig. 4b), indicating that most Ca^{2+} sensors do not reach the fully occupied state during single presynaptic action potentials. This conclusion agrees with the finding at this synapse[14] that increasing the extracellular Ca^{2+} concentration leads to marked potentiation of EPSC amplitudes. The non-saturation of the Ca^{2+} sensors during an action potential and the high intracellular Ca^{2+} cooperativity of vesicle fusion (Fig. 3a) render small changes in amplitude or time course of the local $[Ca^{2+}]_i$ signal very effective in modulating the amount of transmitter output at a synapse. Such changes in the local $[Ca^{2+}]_i$ signal are probably involved in presynaptic inhibition of transmitter release[25] as well as in Ca^{2+}- and activity-dependent forms of synaptic plasticity[26].

Note added in proof: A similar relationship between transmitter release and $[Ca^{2+}]_i$ has recently been reported using Ca^{2+} uncaging by laser photolysis[31]. □

Methods

Tissue preparation, electrophysiological recordings and solutions

We prepared transverse brainstem slices 200 μm thick from 8–10-day-old Wistar rats[6,7,14]. Whole-cell voltage-clamp recordings were done with a double patch-clamp amplifier (EPC-9/2, HEKA elektronik) from presynaptic calyces and postsynaptic principal neurons. The holding potential was −80 mV, and pre- and postsynaptic series resistances were compensated up to 80%. For action potential stimulation of calyces, only the postsynaptic cell was recorded (Fig. 4), and afferent fibres were stimulated with a bipolar electrode. The extracellular solution was a standard Ringer solution[14] with 2 mM $CaCl_2$ and 1 mM $MgCl_2$, to which 10 mM tetraethylammonium (TEA), 0.5 μM tetrodotoxin, 50 μM D-2-amino-5-phophonovaleric acid and 100 μM CTZ were added during paired recordings to suppress undesired current components and desensitization of AMPA receptors[11,12]. Postsynaptic pipette (intracellular) solutions were as described[14]. Presynaptic pipette solutions were made as 2× stocks containing (final concentrations in mM) 130 Cs-gluconate, 20 TEA-Cl, 20 HEPES, 5 Na_2ATP and 0.3 Na_2GTP, to which fura-2 FF (Teflabs; 0.1 mM); DM-nitrophen (Calbiochem; 1 or 2 mM), $CaCl_2$ (0.85 or 1.7 mM) and $MgCl_2$ (0.5 or 0.8 mM) were added. For control experiments at 1 mM free intracellular Mg^{2+} (Fig. 3a), 0.1 mM fura-2FF, 5 mM NP-EGTA (Molecular Probes), 4 mM $CaCl_2$, 3.3 mM $MgCl_2$, 2 mM Na_2ATP and 0.3 mM Na_2GTP were added. Experiments were done at room temperature (21–24 °C). Results are reported as mean ± s.d.

Ca^{2+} uncaging and imaging

We used single light pulses (~1.5 ms) from a flash lamp (Rapp Optoelektronik) for photolysis. $[Ca^{2+}]_i$ imaging was resumed 4 ms after the flash trigger (Fig. 1b), by exciting fura-2 FF at 350 nm and 380 nm with a monochromator (TILL-photonics). Pixel binning (8 × 15; see Fig. 1a) was used to allow short exposure times (5 ms), and free $[Ca^{2+}]_i$ was calculated from background-corrected fluorescence ratios of a series of pixels in the calyx region (Fig. 1a). The dissociation constant (10 ± 2 μM; $n = 5$) of the fura-2FF/Ca^{2+} complex was first determined *in vitro*, by using mixtures of $CaCl_2$ and Ca^{2+} buffers (DM-nitrophen plus DPTA or HEGTA). We obtained the calibration constants at nominally 0 $[Ca^{2+}]$ (R_{min}; 10 mM EGTA, 0 $CaCl_2$) and at 10 μM $[Ca^{2+}]$ ($R_{10\mu M}$) by loading calyces with calibration solutions ($n = 4$ each). For $R_{10\mu M}$, the pipette solution contained 10 μM $[Ca^{2+}]_i$ buffered by isoosmolar DPTA (80 mM), and the extracellular solution was a Na^+-free Ringer with 10 μM $[Ca^{2+}]$. $R_{10\mu M}$ was taken at the end of a 200-s recording period at a holding potential of 0 mV. The ratio at a saturating $[Ca^{2+}]$ (R_{max}; 10 mM $CaCl_2$) was taken from *in vitro* measurements. The calibration constants were corrected[10] for changes in DM-nitrophen fluorescence[27] after flashes.

Deconvolution analysis

EPSC current traces were low-pass filtered at 6 kHz and digitized at 20 kHz. Residual series resistance (1.5–3 MΩ) after partial electronic compensation was compensated off-line[28] before display and analysis. This led to increases in current amplitudes of up to 50%, and to small decreases in the rise times of fast EPSCs (Fig. 4). We calculated transmitter release rates from the EPSC and its time derivative according to the equation given in ref. 15, extended by a term for the slowly decaying mEPSC component (E.N. & T. Sakaba, manuscript in preparation). The mEPSC amplitude, the fast and slow decay time constants and the relative contribution of the slow component were set to the average values found from fits of mEPSCs (see text). This deconvolution analysis provides release rates averaged over time windows equal to the time-to-peak of mEPSCs. It assumes that mEPSCs add up linearly; this assumption might be violated in synapses with strong effects of glutamate spillover[12]. However, a detailed analysis (E.N. & T. Sakaba, manuscript in preparation) shows that the effects of build-up of residual glutamate should be small within short times (< 10 ms) after release. Delays (Fig. 3b) were expressed as the time between the triggering of the flash and a level crossing of five released quanta in integrated release rate traces. We analysed times to peak release from double-exponential fits to release rate traces (Fig. 1e). Analyses were done with IgorPro (Wavemetrics).

Kinetic simulations

The $[Ca^{2+}]_i$ time course with flashes (Fig. 3d) was simulated from the measured time course of the flash by numerical integration of a system of differential equations for the implicated Ca^{2+} and Mg^{2+} buffers. We assumed the presence of an endogenous Ca^{2+} buffer with binding capacity (κ) of 40, as determined experimentally at calyces of Held[23]. The binding rate constants of DM-nitrophen, ATP and endogenous Ca^{2+} buffer were as in ref. 29. A different set of binding rate constants for the endogenous Ca^{2+} buffer[30] at constant κ of 40 produced similar results (data not shown). The $[Ca^{2+}]_i$ time course of Fig. 3d was used to drive the kinetic scheme for Ca^{2+} binding and vesicle fusion (Fig. 3e), which was solved numerically. Release rates were obtained by differentiating the accumulation of vesicles in the fused state, assuming a pool of 1,800 vesicles (Fig. 2d).

Received 5 May; accepted 21 July 2000.

1. Adler, E. M., Augustine, G. J., Duffy, S. N. & Charlton, M. P. Alien intracellular calcium chelators attenuate neurotransmitter release at the squid giant synapse. *J. Neurosci.* **11,** 1496–1507 (1991).
2. Llinás, R., Sugimori, M. & Silver, R. B. Microdomains of high calcium concentration in a presynaptic terminal. *Science* **256,** 677–679 (1992).
3. Yamada, W. M. & Zucker, R. S. Time course of transmitter release calculated from simulations of a calcium diffusion model. *Biophys. J.* **61,** 671–682 (1992).
4. Heidelberger, R., Heinemann, C., Neher, E. & Matthews, G. Calcium dependence of the rate of exocytosis in a synaptic terminal. *Nature* **371,** 513–515 (1994).
5. Roberts, W. M. Localization of calcium signals by a mobile calcium buffer in frog saccular hair cells. *J. Neurosci.* **14,** 3246–3262 (1994).
6. Forsythe, I. D. Direct patch recording from identified presynaptic terminals mediating glutamatergic EPSCs in the rat CNS, *in vitro*. *J. Physiol.* **479,** 381–387 (1994).
7. Borst, J. G. G., Helmchen, F. & Sakmann, B. Pre- and postsynaptic whole-cell recordings in the medial nucleus of the trapezoid body of the rat. *J. Physiol.* **489,** 825–840 (1995).
8. Naraghi, M., Müller, T. H. & Neher, E. Two-dimensional determination of the cellular Ca^{2+} binding in bovine chromaffin cells. *Biophys. J.* **75,** 1635–1647 (1998).
9. Thomas, P., Wong, J. G. & Almers, W. Millisecond studies of secretion in single rat pituitary cells stimulated by flash photolysis of caged Ca^{2+}. *EMBO J.* **12,** 303–306 (1993).
10. Heinemann, C., Chow, R. H., Neher, E. & Zucker, R. S. Kinetics of the secretory response in bovine chromaffin cells following flash photolysis of caged Ca^{2+}. *Biophys. J.* **67,** 2546–2557 (1994).
11. Yamada, K. A. & Tang, C.-M. Benzothiazides inhibit rapid glutamate receptor desensitization and enhance glutamatergic synaptic currents. *J. Neurosci.* **13,** 3904–3915 (1993).
12. Trussell, L. O., Zhang, S. & Raman, I. M. Desensitization of AMPA receptors upon multiquantal neurotransmitter release. *Neuron* **10,** 1185–1196 (1993).
13. Borst, J. G. G. & Sakmann, B. Calcium influx and transmitter release in a fast CNS synapse. *Nature* **383,** 431–434 (1996).
14. Schneggenburger, R., Meyer, A. C. & Neher, E. Released fraction and total size of a pool of immediately available transmitter quanta at a calyx synapse. *Neuron* **23,** 399–409 (1999).
15. van der Kloot, W. Estimating the timing of quantal releases during end-plate currents at the frog neuromuscular junction. *J. Physiol.* **402,** 595–603 (1988).
16. Diamond, J. S. & Jahr, C. E. Asynchronous release of synaptic vesicles determines the time course of the AMPA receptor-mediated EPSC. *Neuron* **15,** 1097–1107 (1995).
17. Wu, L. -G. & Borst, J. G. G. The reduced release probability of releasable vesicles during recovery from short-term synaptic depression. *Neuron* **23,** 821–832 (1999).
18. Dodge, F. A. & Rahamimoff, R. Co-operative action of calcium ions in transmitter release at the neuromuscular junction. *J. Physiol.* **193,** 419–432 (1967).
19. Landò, L. & Zucker, R. S. Ca^{2+} cooperativity in neurosecretion measured using photolabile Ca^{2+} chelators. *J. Neurophysiol.* **72,** 825–830 (1994).
20. Barnes-Davies, M. & Forsythe, I. D. Pre- and postsynaptic glutamate receptors at a giant excitatory synapse in rat auditory brainstem slices. *J. Physiol.* **488,** 387–406 (1995).
21. Lagnado, L., Gomis, A. & Job, C. Continuous vesicle cycling in the synaptic terminal of retinal bipolar cells. *Neuron* **17,** 957–967 (1996).
22. Ohana, O. & Sakmann, B. Transmitter release modulation in nerve terminals of rat neocortical pyramidal cells by intracellular calcium buffers. *J. Physiol.* **513,** 135–148 (1998).
23. Helmchen, F., Borst, J. G. G. & Sakmann, B. Calcium dynamics associated with a single action potential in a CNS presynaptic terminal. *Biophys. J.* **72,** 1458–1471 (1997).
24. Goda, Y. & Südhof, T. Calcium regulation of neurotransmitter release: reliably unreliable? *Curr. Opin. Cell Biol.* **9,** 513–518 (1997).
25. Wu, L. -G. & Saggau, P. Presynaptic inhibition of elicited neurotransmitter release. *Trends Neurosci.* **20,** 204–212 (1997).
26. Zucker, R. S. Calcium- and activity-dependent synaptic plasticity. *Curr. Opin. Neurobiol.* **9,** 305–313 (1999).
27. Zucker, R. S. Effects of photolabile calcium chelators on fluorescent calcium indicators. *Cell Calcium* **13,** 29–40 (1992).
28. Traynelis, S. F. Software-based correction of single compartment series resistance errors. *J. Neurosci. Methods* **86,** 25–34 (1998).
29. Xu, T., Naraghi, M., Kang, H. & Neher, E. Kinetic studies of Ca^{2+} binding and Ca^{2+} clearance in the cytosol of adrenal chromaffin cells. *Biophys. J.* **73,** 532–545 (1997).
30. Xu-Friedman, M. A. & Regehr, W. G. Presynaptic strontium dynamics and synaptic transmission. *Biophys. J.* **76,** 2029–2042 (1999).
31. Bollmann, J. H., Sakmann, B. & Borst, J. G. G. Calcium sensitivity of glutamate release in a calyx-type terminal. *Science* (in the press).

Acknowledgements

We thank T. Sakaba for discussions, and J. Rettig, M. Casado, P. Ascher and R. Fernández-Chacon for critical comments on the manuscript. This work was supported by the Deutsche Forschungsgemeinschaft.

Correspondence and requests for materials should be addressed to R.S. (e-mail: rschneg@gwdg.de).

SLAM (CDw150) is a cellular receptor for measles virus

Hironobu Tatsuo*, Nobuyuki Ono*, Kotaro Tanaka & Yusuke Yanagi

Department of Virology, Faculty of Medicine, Kyushu University, Fukuoka 812-8582, Japan
** These authors contributed equally to this work*

Measles virus continues to be a major killer of children, claiming roughly one million lives a year[1]. Measles virus infection causes profound immunosuppression, which makes measles patients susceptible to secondary infections accounting for high morbidity and mortality[2]. The Edmonston strain of measles virus, and vaccine strains derived from it, use as a cellular receptor human CD46 (refs 3, 4), which is expressed on all nucleated cells; however, most clinical isolates of measles virus cannot use CD46 as a receptor[5]. Here we show that human SLAM (signalling lymphocyte-activation molecule; also known as CDw150), a recently discovered membrane glycoprotein expressed on some T and B cells[6], is a cellular receptor for measles virus, including the Edmonston strain. Transfection with a human SLAM complementary DNA enables non-susceptible cell lines to bind measles virus, support measles virus replication and develop cytopathic effects. The distribution of SLAM on various cell lines is consistent with their susceptibility to clinical isolates of measles virus. The identification of SLAM as a receptor for measles virus opens the way to a better understanding of the pathogenesis of measles virus infection, especially the immunosuppression induced by measles virus.

A marmoset B-cell line transformed with Epstein–Barr virus (EBV), B95-8, and its adherent subline B95a are highly sensitive to measles virus (MV) present in clinical specimens[7]; and strains isolated in B95a cells, but not in Vero (monkey fibroblast) cells, retain pathogenicity for monkeys[7,8]. Thus, B95a is now commonly used to isolate MV from clinical specimens. Unlike the Edmonston strain, which is capable of infecting all $CD46^+$ primate cell lines, MV strains isolated in B95a or other human B-cell lines infect only some primate B-cell and T-cell lines[7,9–14]. By using vesicular stomatitis virus (VSV) pseudotypes bearing MV envelope proteins, we showed that virus entry is a principal determinant of cell tropism of MV strains[14]. Thus, the receptor molecule that enables B95a-isolated MV strains to enter cells appears to be present on a restricted number of lymphoid cell lines. To identify this receptor, we carried out functional expression cloning using the pseudotype system in which the recombinant VSV containing the green fluorescent

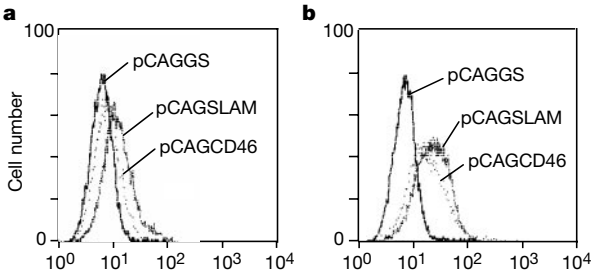

Figure 1 Measle virus binding to CHO cells expressing SLAM or CD46. CHO cells were transiently transfected with pCAGGS, pCAGSLAM or pCAGCD46. The efficiency of transfection was usually more than 50% as determined by flow cytometry analysis. The transfected cells were incubated with the KA (**a**) or Edmonston (**b**) strain of MV for 30 min. After washing, the cells were incubated with a monoclonal antibody specific for MV H protein and stained with FITC-labelled anti-mouse IgG.